

THE HIGH-FREQUENCY ANTIFERROMAGNETIC RESONANCE BRANCH IN CsMnF₃

A. S. BOROVIK-ROMANOV, B. Ya. KOTYUZHANSKIĬ, and L. A. PROZOROVA

Institute for Physics Problems, U.S.S.R. Academy of Sciences

Submitted December 30, 1969

Zh. Eksp. Teor. Fiz. 58, 1911–1918 (June, 1970)

A high-frequency AFMR branch is found in the hexagonal antiferromagnet CsMnF₃ and the size of the gap for this branch is determined. At high temperatures the temperature dependence of the gap is described by the Brillouin function. The temperature dependence of the AFMR line width is also investigated. The AFMR spectrum for CsMnF₃ is calculated on the basis of an expression for the thermodynamic potential satisfying the crystal symmetry.

LEE, Portis, and Witt^[1] have studied the magnetic properties of CsMnF₃ and have found that below T_N = 53.6°K this substance is an antiferromagnet with anisotropy of the “easy plane” type. They observed antiferromagnetic resonance (AFMR) at ν = 9.4 GHz, representing the low-frequency branch of the AFMR spectrum. Several workers^[2-4] have carefully investigated the hyperfine interaction in CsMnF₃ and have performed experiments on nuclear and nuclear-antiferromagnetic double resonance.

We know that in antiferromagnets of the “easy plane” type the exchange branches (ν ∞ H_E) should be accompanied by both a low-frequency (ν ∞ H) and a high-frequency (ν ∞ √2H_AH_E) branch. The high-frequency AFMR branch has previously been observed only in α-Fe₂O₃ and MnCO₃, which contain s-state magnetic ions. Here the spin-orbit interaction is small and the anisotropy energy is determined mainly by the dipole interaction. Since CsMnF₃ also possesses s-state magnetic ions, we can expect that its anisotropy energy will also be so small that its high-frequency resonance branch will be found in the 100–200-GHz region. The present work was undertaken to detect and investigate the high-frequency AFMR branch in CsMnF₃.

CALCULATION OF THE AFMR SPECTRUM

CsMnF₃ is a hexagonal crystal with symmetry that is described by the D_{6h}⁴ space group.^[5] Its unit cell (Fig. 1) contains six Mn²⁺ ions occupying the following crystallographic sites: Mn I—(0, 0, 0) and (0, 0, 1/2); Mn II—(1/3, 2/3, u), (1/3, 2/3, 1/2 - u), (2/3, 1/3, 1/2 + u), and (2/3, 1/3, -u).

We first determine the possible magnetic structures in CsMnF₃, following Dzyaloshinskiĭ.^[6] We denote the magnetic moments of Mn I ions by s₁ and s₂, respectively, and the magnetic moments of Mn II ions by σ₁, σ₂, σ₃, and σ₄; we introduce the following combinations:

$$\begin{aligned} l_1 &= s_1 - s_2, & m_1 &= s_1 + s_2, \\ l_2 &= -\sigma_1 + \sigma_2 + \sigma_3 - \sigma_4, & l_3 &= -\sigma_1 - \sigma_2 + \sigma_3 + \sigma_4, \\ l_4 &= -\sigma_1 + \sigma_2 - \sigma_3 + \sigma_4, & m_2 &= \sigma_1 + \sigma_2 + \sigma_3 + \sigma_4. \end{aligned} \tag{1}$$

The components of the vectors l_α and m_α are the bases of irreducible representations of the D_{6h}⁴ group, which is here derived from the D_{6h}⁴ group by assuming that all translations are identical elements. By comparing the characters of these representations with those of the D_{6h} point group^[7] we obtained the accom-

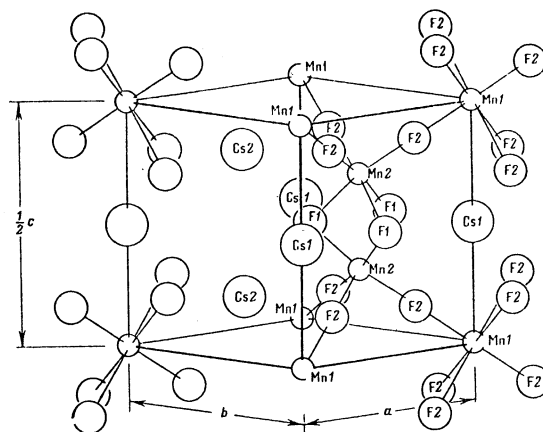


FIG. 1. Half of a CsMnF₃ unit cell.

panying table, which gives the representations of the transformations for each of the l_{αi} and m_{αi} components (using the notation of^[7]).

Following the thermodynamic theory of second-order phase transitions,^[8,6] we can now write a general expression for the thermodynamic potential Φ based on the crystal symmetry but limited to second-order terms. It must be remembered that second-order invariants can be composed only of quantities transforming according to a single representation. We have

$$\begin{aligned} \Phi &= \frac{1}{2}A_1l_1^2 + \frac{1}{2}A_2l_2^2 + C_1l_2 + \frac{1}{2}A_3l_3^2 + \frac{1}{2}A_4l_4^2 \\ &+ \frac{1}{2}B_1m_1^2 + \frac{1}{2}B_2m_2^2 + Dm_1m_2 + \frac{1}{2}a_1l_1^2 + \frac{1}{2}a_2l_2^2 \\ &+ cl_2l_2 + \frac{1}{2}a_3l_3^2 + \frac{1}{2}a_4l_4^2 + \frac{1}{2}b_1m_1^2 \\ &+ \frac{1}{2}b_2m_2^2 + dm_1m_2 - mH. \end{aligned} \tag{2}$$

The magnetic structures that can be formed in a crystal as a result of a second-order phase transition from the paramagnetic state are determined by the irreducible representations of the crystallographic class.^[8,6] We introduce the following notation for the different types of magnetic moment ordering in CsMnF₃: F₁—ferromagnetic ordering of the Mn I magnetic moments, F₂—the same for Mn II; A_α—antiferromagnetic ordering of the Mn I magnetic moments; A_α the same for Mn II with spin alternation corresponding to l_α ≠ 0. The indices || and ⊥ indicate the spin directions relative to the z axis. Any magnetic structure can be represented as a combination of the F's and A's. The last column of the table gives the magnetic structures that can exist in crystals with D_{6h}⁴ symmetry. The table shows that

| Vector components | Representations | Type of magnetic structure | Vector components | Representations | Type of magnetic structure |
|----------------------------------|-----------------|----------------------------|-------------------|-----------------|----------------------------|
| m_{1z}, m_{2z} | A_{2g} | $(F_1 + F_2)_{\parallel}$ | l_{3z} | B_{1u} | $A_{2\parallel}$ |
| $m_{1x}, m_{1y}; m_{2x}, m_{2y}$ | E_{1g} | $(F_1 + F_2)_{\perp}$ | l_{3x}, l_{3y} | E_{2u} | $A_{2\perp}$ |
| l_{1z}, l_{2z} | B_{2g} | $(A_1 + A_2)_{\parallel}$ | l_{4z} | A_{1u} | $A_{4\parallel}$ |
| $l_{1x}, l_{1y}; l_{2x}, l_{2y}$ | E_{2g} | $(A_1 + A_2)_{\perp}$ | l_{4x}, l_{4y} | E_{1u} | $A_{4\perp}$ |

weak ferromagnetism is theoretically impossible in CsMnF_3 . Also, the Mn I and Mn II magnetic moments can be ordered simultaneously only when the directional alternation of the Mn II magnetic moments corresponds to $l_2 \neq 0$.

The available experimental data^[1] provide a basis for the hypothesis that below $T_N = 53.6^\circ\text{K}$ the magnetic moments of both Mn groups are ordered. Otherwise the disordered system would be responsible for a steep rise of the susceptibility with decreasing temperature; this effect is not observed experimentally. We can therefore assume that magnetic structure of the $A_1 + A_2$ type is realized in CsMnF_3 . The identical susceptibilities along and perpendicular to the z axis, together with the observation of the low-frequency AFMR branch, indicate that the spins lie in the basal plane of the crystal. Therefore we shall assume henceforth that $l_3 = l_4 = 0$ and $l_{1z} = l_{2z} = 0$. It is indicated by data in^[3] that in good CsMnF_3 single crystals in-plane anisotropy does not exist, and that the vectors \mathbf{I}_1 and \mathbf{I}_2 are perpendicular to the applied field \mathbf{H} . We shall assume that the magnetic field is applied along the x and z axes, that \mathbf{I}_1 and \mathbf{I}_2 are parallel to the y axis, and that $l_2 = 2l_1 = 4M_0$ in accordance with the number of magnetic ions in the sublattices (the magnetization of each sublattice is denoted by M_0).

Writing the Landau-Lifshitz equations for each sublattice, we arrive at the following equations of motion for the magnetic moments:

$$\begin{aligned} -\frac{1}{\gamma} \frac{dl_{\alpha z}}{dt} &= \left[l_{\alpha} \frac{\partial \Phi}{\partial m_{\alpha}} \right] + \left[m_{\alpha} \frac{\partial \Phi}{\partial l_{\alpha}} \right], \\ -\frac{1}{\gamma} \frac{dm_{\alpha}}{dt} &= \left[l_{\alpha} \frac{\partial \Phi}{\partial l_{\alpha}} \right] + \left[m_{\alpha} \frac{\partial \Phi}{\partial m_{\alpha}} \right]. \end{aligned} \quad (3)$$

The Landau-Lifshitz equations presuppose that the magnetic moments of the sublattices have constant moduli:

$$l_{\alpha}^2 + m_{\alpha}^2 = \text{const}, \quad (4)$$

so that the thermodynamic potential (2) can be written as

$$\Phi = \frac{1}{2} B_1 m_1^2 + \frac{1}{2} B_2 m_2^2 + C l_1 l_2 + D m_1 m_2 + \frac{1}{2} a_1 l_1^2 + \frac{1}{2} a_2 l_2^2 + c l_1 l_2 z + \frac{1}{2} b_1 m_1^2 z + \frac{1}{2} b_2 m_2^2 z + d m_1 m_2 z - m_1 H - m_2 H. \quad (5)$$

Assuming $dl_{\alpha}/dt = dm_{\alpha}/dt = 0$ and $(m_{\alpha} l_{\alpha}) = 0$, from (3) and (5) we obtain equations for the dependences of m_1 and m_2 on the field applied in a plane perpendicular to z:

$$m_1 = \frac{B_2 - \frac{1}{2}C - D}{\Delta_1^2} H, \quad m_2 = \frac{B_1 - 2C - D}{\Delta_1^2} H; \quad (6)$$

$$\Delta_1^2 = B_1 B_2 + C^2 - D^2 - (\frac{1}{2} B_1 + 2B_2)C.$$

The total magnetization is therefore

$$m_{\perp} = \frac{B_1 + B_2 - 2D - \frac{5}{2}C}{\Delta_1^2} H. \quad (7)$$

When the field is along the z axis we have

$$m_1 = \frac{(B_2 - \frac{1}{2}C - D) + b_2 - d}{\Delta_2^2} H, \quad m_2 = \frac{(B_1 - 2C - D) + b_1 - d}{\Delta_2^2} H; \quad (8)$$

$$m_{\parallel} = \frac{(B_1 + B_2 - 2D - \frac{5}{2}C) + b_1 + b_2 - 2d}{\Delta_2^2} H, \quad (9)$$

where

$$\Delta_2^2 = [B_1 B_2 + C^2 - D^2 - (\frac{1}{2} B_1 + 2B_2)C] + b_1 (B_2 - \frac{1}{2}C + \frac{1}{2} b_2) + b_2 (B_1 - 2C + \frac{1}{2} b_1) - 2Dd - d^2.$$

It is now convenient to introduce the effective field

$$H_E = \frac{3M_0 \Delta_1^2}{B_1 + B_2 - 2D - \frac{5}{2}C}. \quad (10)$$

Then

$$m_{\perp} = \frac{3M_0}{H_E} H, \quad m_{\parallel} = \frac{3M_0}{H_E} H(1 + \epsilon), \quad (11)$$

where ϵ is of the order of the ratio between relativistic terms and exchange terms, i.e., $\epsilon \ll 1$. From (3) we obtain, to terms of the order H_A/H_E , the following expressions for the AMFR frequencies when $\mathbf{H} \parallel z$:

$$v_1 / \gamma = 0, \quad (12)$$

$$(v_2 / \gamma)^2 = 2H_A H_E + H^2 = H_{AE}^2 + H^2, \quad (13)$$

$$(v_3 / \gamma)^2 = 4C[5C + 4D - 2(B_1 + B_2)]M_0^2 + f_1(H^2), \quad (14)$$

$$(v_4 / \gamma)^2 = 4C[5C + 4D - 2(B_1 + B_2)]M_0^2 + f_2(H^2), \quad (15)$$

where $H_A = \frac{2}{3}(a_1 + 4a_2 + 4c)M_0$. When $\mathbf{H} \perp z$ the first branch changes greatly and we obtain

$$(v_1 / \gamma)^2 = H^2. \quad (16)$$

The magnetic field dependence disappears in the remaining branches.

In^[4] the AFMR spectrum was calculated using the molecular field model and taking only nearest-neighbor interactions into account. This procedure leads to the following relations between the coefficients of the thermodynamic potential:

$$B_1 = 0, \quad B_2 = \lambda_2 / 4, \quad D = -C = \lambda_1 / 4, \quad (17)$$

where in the expression for the energy λ_1 is the coefficient of the $s_{\alpha} s_{\beta}$ terms and λ_2 is the coefficient of the $\sigma_{\alpha} \sigma_{\beta}$ terms. Then (13)–(15) are transformed as follows:

$$\left(\frac{v_2}{\gamma} \right)^2 = 6 \frac{\lambda_1 \lambda_2}{\lambda_1 + \lambda_2} M_0 H_A + H^2, \quad (13a)$$

$$(v_3 / \gamma)^2 = \frac{1}{4} \lambda_1 (\lambda_1 + 2\lambda_2) M_0^2 + f_1(H^2), \quad (14a)$$

$$(v_4 / \gamma)^2 = \frac{1}{4} \lambda_1 (\lambda_1 + 2\lambda_2) M_0^2 + f_2(H^2). \quad (15a)$$

In his final equations Welsh^[4] assumed $\lambda_1 = \lambda_2$; then our expressions for the gaps in the spectrum coincide with his results. However a different field dependence is obtained for the second branch (Welsh gives $\frac{3}{4}H^2$).

We must also discuss the anisotropy energy further. The expression (2) for the thermodynamic potential contains all the anisotropy energy terms that are permitted by the CsMnF_3 crystal symmetry. Equations (13) and (9) show that the magnitude of the gap for the second

branch of the spectrum depends on a combination of the constants a_1 , a_2 , and c , while the anisotropy of the magnetic susceptibility is determined by a combination of the constants b_1 , b_2 , and d . Terms such as $s_{1Z}s_{2Z}$, $\sigma_{\alpha Z}\sigma_{\beta Z}$, and $s_{\alpha Z}\sigma_{\beta Z}$ have been omitted from the expression for the energy in^[1,4]. Therefore the results given there involve only a single anisotropy field in both the susceptibility anisotropy and the expression for the gap.

Since we are primarily interested in the high-frequency AFMR branch we have not considered the influence of the nuclear system on AFMR; this aspect has been studied in detail by Welsh.^[4]

EXPERIMENTAL PROCEDURE AND SAMPLES

AFMR in CsMnF_3 was investigated with the magnetic spectrometer described in^[9]. The resonance absorption line was recorded through two-coordinate automatic registration of the variation of the microwave signal reflected from the crystal as a function of the magnetic field H .

The measurements were obtained for the 2° – 65°K range. Above 4.2°K we used a vacuum cryostat^[10] with a carbon adsorption pump. Temperatures were measured with a carbon thermometer calibrated at 2.1, 4.2, 14.0, 20.39, 27.25, 62.8, and 77.5°K . The measurement accuracy and the stability of the temperatures were maintained within 0.3°K .

The CsMnF_3 single crystals were grown in a helium atmosphere by S. V. Petrov, using the Stockbarger method and the apparatus described in^[11]. After the CsMnF_3 single crystals were x-ray oriented they were cut in the form of parallelepipeds. Our basic measurements were performed on a $1.6 \times 0.8 \times 0.2$ -mm sample having large faces that coincided with the basal plane to within 5° . The samples were mounted with BF-6 cement on the copper end cap of the waveguide.

EXPERIMENTAL RESULTS

1. The High-frequency Resonance Branch at $T = 4.2^\circ\text{K}$

With the basal plane of the sample perpendicular to the magnetic field, we observed an absorption line corresponding to the high-frequency branch of the AFMR spectrum. At $T = 4.2^\circ\text{K}$ we carefully investigated the dependence of the high-frequency branch on the magnetic field. Figure 2 shows that our results agree well with (13) when we insert the values

$$H_{AE} = 41.1 \pm 0.6 \text{ kOe}, \quad \gamma_0 = 2.8 \text{ kOe/GHz} \quad (g = 2.0).$$

Our value of γ agrees with^[1,4] and is the result usually obtained for compounds with Mn^{++} ions. No other spectral branches were observed up to ~ 190 GHz.

2. Temperature Dependence of the Gap in the High-Frequency AFMR branch

The temperature dependence of the resonance field was studied at several fixed frequencies. With increasing temperature the absorption line shifted towards higher magnetic fields. The paramagnetic transition temperature T_N was defined as the point at which the resonance field ceased to vary with heating of the sam-

ple. Our measurements yielded $T_N = 53.6 \pm 0.3^\circ\text{K}$, in agreement with^[11].

It should be noted that in our experiments the transition point was determined at ~ 40 kOe and can therefore, as shown in^[12], differ from T_N in zero field by the amount

$$\Delta T_N = T_N \frac{\Delta \chi_{\perp}}{\chi_{\perp}} \left(\frac{H}{H_E} \right)^2.$$

A calculation shows that in the case of CsMnF_3 this shift of T_N does not exceed 0.2°K and is thus smaller than our experimental error.

Assuming that the field dependence of the resonance frequency (13) holds true for all temperatures, we calculated $H_{AE}^2(T)$ from the experimental data. The value of H_{AE} extrapolated to 0°K was 41.1 ± 0.6 kOe, which corresponds to the frequency $\nu_0 = 115 \pm 2$ GHz. Figure 3 shows the temperature dependence of the squared relative value of the gap. The experimental spread of H_{AE}^2 was determined by the resonance line width ($\sim 0.1 \Delta H$) and by the inaccuracies of the temperature measurements.

3. Temperature Dependence of the Line Width

Since the field dependence of the AFMR frequency is nonlinear, the experimental values of the half-width ΔH were converted to equivalent line widths by means of the expression

$$\Delta \nu = \frac{\gamma^2 H}{\nu} \Delta H.$$

Figure 4 shows the temperature dependence of $\Delta \nu$. We observe that $\Delta \nu$ increases rapidly as the transition temperature is approached, but then dips sharply at a temperature 2° below T_N , after which it remains constant. The result $\Delta \nu_2 \approx 0.8$ GHz obtained for the high-frequency branch at helium temperatures is close to the value of $\Delta \nu_1 (\approx 0.3$ GHz) that was obtained for the low-frequency branch in the same crystal measured at 94 GHz.

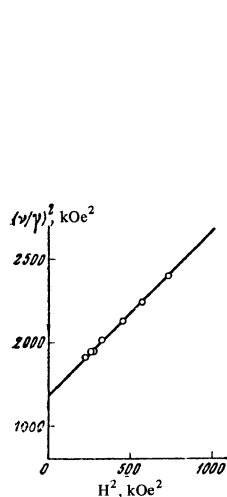


FIG. 2

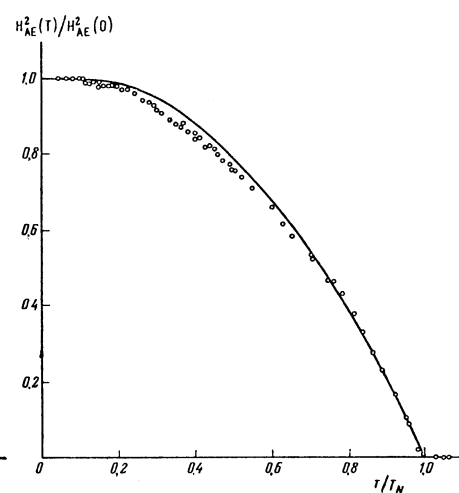


FIG. 3

FIG. 2. Dependence of the resonance frequency of the high-frequency branch on the applied magnetic field.

FIG. 3. Temperature dependence of the square of the relative gap magnitude and a comparison with the square of the reduced Brillouin function $B_{3/2}^2(T/T_N)$ (continuous line).

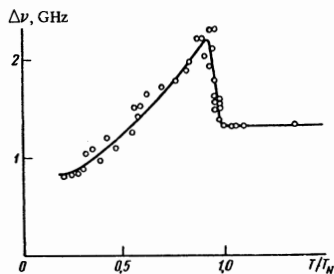


FIG. 4. Temperature dependence of the line width for the high-frequency branch.

DISCUSSION OF RESULTS

Utilizing the statistical measurements in^[1] together with our value for H_{AE} at $T = 0^\circ\text{K}$, we calculated the anisotropy field with the aid of (13) and (11):

$$H_A = H_{AE}^2 / 2H_E = 2.48 \pm 0.07 \text{ kOe.}$$

A value of the anisotropy field was derived in^[1]; where H_A was determined experimentally from the magnetic susceptibility anisotropy measured parallel and perpendicular to the z axis. However, as already mentioned, this anisotropy field does not appear in the equation for the gap in AFMR. There is therefore no basis for comparing these values. The single-ion anisotropy field H_A^{cryst} and the contribution to the anisotropy field from the dipolar interaction (H_A^{dip}) were also calculated in^[1]:

$$H_A^{(\text{cryst.})} = 1.17 \text{ kOe, } H_A^{(\text{dip.})} = 6.80 \text{ kOe.}$$

We here obtain a value of H_A that considerably exceeds our experimental value, possibly because of the extreme simplifications used in^[1].

In Fig. 3 the experimental dependence of H_{AE}^2 is compared with the square of the Brillouin function for $s = 5/2$ (the continuous curve). At high temperatures the experimental points are well fitted by the curve. We therefore conclude that at high temperatures the anisotropy energy $K_{\perp} = \chi_{\perp} / H_{AE}^2$ is proportional to the square of the magnetization of the sublattices. This result indicates that the anisotropy energy receives its main contribution from the dipolar energy. At low temperatures our experiments are insufficiently accurate for any comparison with current spin-wave theories.

A very interesting result, for which we can propose no reasonable explanation, consists in the fact that the peak of the line-width temperature dependence is not located at the transition temperature.

The authors are indebted to P. L. Kapitza for his interest. We also thank I. E. Dzyaloshinskiĭ for valuable suggestions and discussions, S. V. Petrov for growing the CsMnF_3 crystals, G. É. Karstens and A. G. Bol'shakov for the x-ray study and orientation of the crystals, and K. I. Rassokhin for experimental assistance.

¹K. Lee, A. M. Portis, and G. L. Witt, Phys. Rev. **132**, 144 (1963).

²G. L. Witt and A. M. Portis, Phys. Rev. **136**, A1316 (1964).

³V. Minkiewicz and A. Nakamura, Phys. Rev. **143**, 361 (1966).

⁴L. B. Welsh, Phys. Rev. **156**, 370 (1967).

⁵Internationale Tabellen zur Bestimmung von Krystallstrukturen, Vol. 1, Gebrüder Borntraeger, Berlin, 1935.

⁶I. E. Dzyaloshinskiĭ, Zh. Eksp. Teor. Fiz. **32**, 1547 (1957) [Sov. Phys.-JETP **5**, 1259 (1957)].

⁷L. D. Landau and E. M. Lifshitz, *Quantovaya mekhanika* (Quantum Mechanics), Fizmatgiz, 1963.

⁸L. D. Landau and E. M. Lifshitz, *Statisticheskaya fizika* (Statistical Physics), Nauka, 1964.

⁹G. D. Bogomolov, Yu. F. Igonin, L. A. Prozorova, and F. S. Rusin, Zh. Eksp. Teor. Fiz. **54**, 1069 (1968) [Sov. Phys.-JETP **27**, 572 (1968)].

¹⁰L. A. Prozorova and A. S. Borovik-Romanov, Zh. Eksp. Teor. Fiz. **55**, 1727 (1968) [Sov. Phys.-JETP **28**, 910 (1968)].

¹¹N. N. Mikhaĭlov and S. V. Petrov, *Kristallografiya* **11**, 443 (1966) [Sov. Phys. Crystallogr. **11**, 390 (1966)].

¹²A. S. Borovik-Romanov, *Itogi nauki, seriya Fiz.-mat. nauki* **4**, Acad. Sci. USSR, 1962.